Electrohydrodynamic convection in liquid crystals driven by multiplicative noise: Sample stability

Ulrich Behn,[1] Adrian Lange,[2] and Thomas John[1]
[1]*Institut für Theoretische Physik, Universität Leipzig, Augustusplatz 10, D-04109 Leipzig, Germany*
[2]*Theoretical Physics, University of Oxford, 1 Keble Road, Oxford OX1 3NP, United Kingdom*
and Institut für Theoretische Physik, Universität Magdeburg, P.O.B. 4120, D-39016 Magdeburg, Germany
(Received 18 April 1997; revised manuscript received 26 March 1998)

We study the stochastic stability of a system described by two coupled ordinary differential equations parameterically driven by dichotomous noise with finite correlation time. For a given realization of the driving noise (a sample), the long time behavior is described by an infinite product of random matrices. The transfer matrix formalism leads to a Frobenius-Perron equation, which seems not solvable. We use an alternative method to calculate the largest Lyapunov exponent in terms of generalized hypergeometric functions. At the threshold, where the largest Lyapunov exponent is zero, we have an exact analytical expression also for the second Lyapunov exponent. The characteristic times of the system correspond to the inverse of the Lyapunov exponents. At the threshold the first characteristic time diverges and is thus well separated from the correlation time of the noise. The second time, however, depending on control parameters, may reach the order of the correlation time. We compare the corresponding threshold with a threshold from a simple mean-field decoupling and with the threshold describing stability of moments. The different stability criteria give similar results if the characteristic times of the system and the noise are well separated, the results may differ drastically if these times become of similar order. Digital simulation strongly confirms the criterion of sample stability. The stochastic differential equations describe in the frame of a simple one-dimensional model and a more realistic two-dimensional model the appearance of normal rolls in nematic liquid crystals. The superposition of a deterministic field with a ''fast'' stochastic field may lead to stable region that extends beyond the threshold values for deterministic or stochastic excitation alone, forming thus a stable tongue in the space of control parameters. For a certain measuring procedure the threshold curve may appear discontinuous as observed previously in experiment. For a different set of material parameters the stable tongue is absent.
[S1063-651X(98)14508-7]

PACS number(s): 61.30.−v, 47.20.−k, 47.65.+a, 05.40.+j

I. INTRODUCTION

The influence of stochastic modulation of parameters in spatially extended systems is a subject of recent interest [1]. Especially well investigated are electrohydrodynamic instabilities in nematic liquid crystals sandwiched between two parallel electrodes where the convection is driven by an external (spatially homogeneous) time dependent stochastic electric field. The electric field is the superposition of a ''slow'' (harmonically modulated or constant) deterministic component and a ''fast'' stochastic component [2–10]. Slow and fast refer to the characteristic times of the liquid crystal describing the relaxation of space charge and director in absence of external electric fields.

In experiments [2–7] it was found that the superposition of a fast stochastic field increases the threshold for the deterministic field (i.e., stabilizes the homogeneous state) up to a certain critical value of the stochastic field. Beyond this value the homogeneous, i.e., undistorted, state is unstable, which leads to a discontinuous behavior of the threshold curve as a function of the stochastic field.

Theoretically, this phenomenon found—at least qualitatively—an explanation [8–11] by considering the stability of moments (the stochastic averages of space charge and director). This theory explained qualitatively (i) the discontinuous behavior of the threshold at a critical strength of the noise, (ii) the change from discontinuous to continuous behavior of the threshold with increasing characteristic time of the noise, and (iii) the change from a stabilizing to a destabilizing effect of the noise if its correlation time becomes comparable to the characteristic times of the system. The quantitative agreement was, however, not satisfactory. It remained an open question whether the quantitative discrepancies were the result of the approximate treatment of the nemato-electrohydrodynamic equations, of poor knowledge of material parameters, of the choice of the stochastic stability criterion, or depending on other reasons.

There exist different criteria for stochastic stability [12–15] based, for example, on the stability of (first or higher) moments, on the bifurcation of the most probable value, or on the concept of sample stability describing the stability of one stochastic trajectory (a sample).

In this paper, we consider sample stability within a simple one-dimensional model describing the stability of the undistorted state in a simplified geometry and neglecting boundary conditions. We calculate analytically the corresponding Lyapunov exponent λ and compare the threshold obtained by solving $\lambda = 0$ with thresholds obtained from different criteria and the results of a numerical simulation of stochastic trajectories. The simulation—independent of any theoretical formalism—strongly confirms the concept of sample stability. We discuss under what conditions different criteria give similar or different results. We further give results for a two-

dimensional model that is more realistic in the determination of the characteristic length of the pattern by mode selection.

From the formal point of view, the exact treatment of the stochastic dynamics leads to the problem of determining properties of infinite products of random matrices. This notoriously difficult problem [16] appears also in a number of different fields in statistical physics and is a subject of recent interest, cf. [17–25]. A comprehensive review is given in [26]. As a spin-off, in this paper we obtain an analytic result for the largest Lyapunov exponent describing the stability of a dynamical system related to a new class of infinite products of random matrices. For this class of matrices one of the standard methods, the transfer matrix formalism, leads to a Frobenius-Perron equation, which, to the best of our knowledge, has not hitherto been solved.

In the one-dimensional version, the nemato-electrohydrodynamic equations describing the stability of the undistorted state in a thin layer in the middle between the electrodes against the formation of roll cells reduce to the nonautonomous system [27–29]

$$\dot{\vec{z}} = \mathbf{C}(t)\vec{z}, \tag{1.1}$$

where $\vec{z} = (q, \psi)^T$ and

$$\mathbf{C}(t) = -\begin{pmatrix} 1 & \zeta\varepsilon_t \\ \zeta\varepsilon_t & \varepsilon_0^2 + \varepsilon_t^2 \end{pmatrix}. \tag{1.2}$$

The variables q and ψ describe space charge and spatial variation of the angle between director and electrode plane in dimensionless units, respectively. The undistorted state is characterized by $\vec{z} = 0$. ε_t is the external time dependent electric field in dimensionless units. The time is scaled in units of the relaxation time of the space charges. ζ is a material parameter. ε_0 is proportional to the wave number of the rolls normally to be determined by mode selection. As typical for one-dimensional models it is impossible to select a mode of a characteristic length determined essentially by the sample thickness; the corresponding wave number in the conductive mode is set *by hand* to π/d. For the dielectric mode the wave number is an order of magnitude larger and essentially determined by bulk properties, so that mode selection works even in the one-dimensional model [28,30].

The two-dimensional version [11,30–33] contains explicitly the distance d between the electrodes as a parameter and thus allows one to determine also the wave number of the rolls in the conductive regime by mode selection. The equations are—in principle—similar to the one-dimensional version but much more difficult to handle since quite a number of parameters are involved depending on material properties *and* on the wave number of the rolls. This makes an analytic treatment, such as it is possible for the one-dimensional version, into a hopeless enterprise. Therefore we present first an almost thorough analytic study of the one-dimensional version and then the numerical results for the two-dimensional version. The thresholds in both models show qualitatively the same behavior and differ by less than 10%. The wave numbers may differ in a more significant way.

We investigate the superposition of a constant deterministic field ε_1 and a stochastic field, modeled by the dichotomous Markov process (DMP) $\varepsilon_t^{\mathrm{DMP}}$, which takes with equal probability the two values $\sigma\varepsilon$, $\sigma = \pm$. Thus ε_t takes values $\varepsilon_\sigma = \varepsilon_1 + \sigma\varepsilon$. For a given realization ε_σ of the DMP, $\mathbf{C}(t)$ takes the constant values $\mathbf{C}^\sigma$, $\sigma = \pm$, with obvious definition. The DMP is the simplest discrete Markovian process with finite correlation time and is easily generated in experiment. Its autocorrelation decays exponentially, $\langle \varepsilon_t \varepsilon_{t'} \rangle = \varepsilon^2 \exp[-2\alpha(t-t')]$. The parameter α determines the inverse correlation time and describes the mean number of jumps in unit time.

Note that Eq. (1.2) contains the *square* of the stochastic field. This forces us—from the formal side—to consider a process with a finite correlation time. From the physical side, we are also forced to consider a process with a finite correlation time. This is because one of the characteristic times of the system decreases with increasing field and may reach the order of the characteristic time of the noise so that the idealization of white noise should fail.

Theoretically, the concept of sample stability is applicable to any linear stochastic system of first order differential equations with a quadratic coefficient matrix [13]. From the practical point of view, however, the explicit evalution of the simplest nontrivial case of a 2×2 system driven by dichotomous noise needs considerable effort. The step from pure stochastic excitation considered in [10] to the case of a superposition of constant and stochastic excitation investigated here is not a simple exercise.

The paper is organized as follows. In the next section we derive the formal solution of Eq. (1.1) for a given realization of the driving noise which—in the long time limit—leads to an infinite product of random matrices. To illustrate the difficulty in calculating the largest Lyapunov exponent of this product we consider in Sec. III the transfer matrix formalism and derive the Frobenius-Perron equation. In Sec. IV we use an alternative approach to calculate the Lyapunov exponent analytically in terms of generalized hypergeometric functions. The corresponding sample stability threshold is compared with thresholds obtained from different criteria and results of numerical simulations. Section V contains the results for the two-dimensional version. Details of the analytic evaluation are deferred to Appendix A. In Appendix B the reader finds values of material parameters used in the numerical calculations and the rescaling of dimensionless quantities. Appendix C gives the explicit representation of the coefficients for the two-dimensional model.

II. FORMAL SOLUTION

We derive the formal solution of Eq. (1.1) for a given trajectory of $\varepsilon_t^{\mathrm{DMP}}$ with jumps at times t_ν, $\nu = 0,1,\ldots,n$, where $t_n > t_{n-1} > \cdots > t_1 > t_0$. Let us first consider a time interval between two jumps and diagonalize $\mathbf{C}^\sigma$. The (real) eigenvalues of $\mathbf{C}^\sigma$ are

$$\lambda_{1/2}^\sigma = -\frac{1+\varepsilon_0^2+\varepsilon_\sigma^2}{2} \pm \sqrt{\frac{1}{4}(1-\varepsilon_0^2-\varepsilon_\sigma^2)^2 + \zeta^2\varepsilon_\sigma^2}. \tag{2.1}$$

We look for a unitary matrix $\mathbf{U}^\sigma$, $\mathbf{U}^\sigma(\mathbf{U}^\sigma)^{-1} = (\mathbf{U}^\sigma)^{-1}\mathbf{U}^\sigma = \mathbf{1}$, which diagonalizes $\mathbf{C}^\sigma$:

$$\mathbf{U}^{\sigma}\mathbf{C}^{\sigma}(\mathbf{U}^{\sigma})^{-1}=\begin{pmatrix}\lambda_1^{\sigma} & 0\\ 0 & \lambda_2^{\sigma}\end{pmatrix}\equiv\mathrm{diag}(\lambda_i^{\sigma}), \tag{2.2}$$

and

$$(\mathbf{U}^{\sigma})^{-1}\mathrm{diag}(\lambda_i^{\sigma})\mathbf{U}^{\sigma}=\mathbf{C}^{\sigma}. \tag{2.3}$$

Note that the eigenvalues $\lambda_{1/2}^{\sigma}$ do not depend on sgn ε_{σ} but $\mathbf{C}^{\sigma}$ does. Therefore, the unitary matrix $\mathbf{U}^{\sigma}$ depends not only on the realization of the DMP but also on sgn ε_{σ}.

We try the general *Ansatz*

$$\mathbf{U}^{\sigma}=\begin{pmatrix}c_{\sigma} & -\rho\sqrt{1-c_{\sigma}^2}\\ \rho\sqrt{1-c_{\sigma}^2} & c_{\sigma}\end{pmatrix}. \tag{2.4}$$

c_{σ} and ρ with $|\rho|=1$ are determined by inserting Eq. (2.4) into Eq. (2.3). $C_{11}^{\sigma}=\lambda_1^{\sigma}c_{\sigma}^2+\lambda_2^{\sigma}(1-c_{\sigma}^2)=-1$ leads to

$$c_{\sigma}^2=-\frac{1+\lambda_2^{\sigma}}{\lambda_1^{\sigma}-\lambda_2^{\sigma}}, \tag{2.5}$$

which generates $C_{22}^{\sigma}=-\varepsilon_0^2-\varepsilon_{\sigma}^2$. $C_{12}^{\sigma}=C_{21}^{\sigma}=(\lambda_2^{\sigma}-\lambda_1^{\sigma})\rho\sqrt{c_{\sigma}^2(1-c_{\sigma}^2)}=-\zeta\varepsilon_{\sigma}$ leads, by exploiting Eq. (2.5) via $-\rho\sqrt{-(1+\lambda_1^{\sigma}+\lambda_2^{\sigma}+\lambda_1^{\sigma}\lambda_2^{\sigma})}=-\rho\sqrt{\zeta^2\varepsilon_{\sigma}^2}=-\rho\zeta|\varepsilon_{\sigma}|$, to

$$\rho=\mathrm{sgn}\ \varepsilon_{\sigma}. \tag{2.6}$$

It is easy to prove that Eq. (2.2) is satisfied. For pure stochastic excitation, i.e., $\varepsilon_1\equiv 0$, Eq. (2.6) reduces to $\rho=\sigma$.

The time evolution between two jumps is now easily obtained. Introducing $\mathbf{U}^{\sigma}\vec{z}=\vec{W}^{\sigma}$ we have from Eq. (1.1)

$$\dot{\vec{W}}^{\sigma}=\mathrm{diag}(\lambda_i^{\sigma})\vec{W}^{\sigma}, \tag{2.7}$$

which is solved by

$$\vec{W}^{\sigma}(t)=\mathrm{diag}\{\exp[\lambda_i^{\sigma}(t-t')]\}\vec{W}^{\sigma}(t'). \tag{2.8}$$

The inverse transformation leads to

$$\vec{z}_{\sigma}(t)=\mathbf{T}^{\sigma}(t-t')\vec{z}_{\sigma}(t'), \tag{2.9}$$

where $\mathbf{T}^{\sigma}$ is the time evolution matrix

$$\mathbf{T}^{\sigma}(\tau)=(\mathbf{U}^{\sigma})^{-1}\mathrm{diag}[\exp(\lambda_i^{\sigma}\tau)]\mathbf{U}^{\sigma}. \tag{2.10}$$

For a given realization of the driving process with jumps at times t_{ν} between the values $\varepsilon_{\sigma_{\nu}}=\varepsilon_1+\sigma_{\nu}\varepsilon$, $\sigma_{\nu}=(-1)^{\nu}\sigma_0$, iteration of Eq. (2.9) gives the formal solution of Eq. (1.1) as

$$\vec{z}_{\sigma_n}(t)=\mathbf{T}^{\sigma_n}(t-t_n)\cdots\mathbf{T}^{\sigma_2}(t_3-t_2)\mathbf{T}^{\sigma_1}(t_2-t_1)\mathbf{T}^{\sigma_0}\times(t_1-t_0)\vec{z}_{\sigma_0}(t_0)\equiv\mathcal{T}^{(n)}(t,\{t_{\nu}\},\sigma_0)\vec{z}_{\sigma_0}(t_0), \tag{2.11}$$

where $\mathcal{T}^{(n)}$ denotes the ordered product of $n+1$ random matrices of type (2.10). The formal solution (2.11) serves as starting point to investigate the stability by numerical simulation.

The stability of the stochastic trajectory (2.11) for a given realization of the driving process (a sample) is determined by the largest Lyapunov exponent of the matrix $\mathcal{T}^{(n)}$ in the limit $n\to\infty$. If this exponent has a positive real part the trajectory diverges, otherwise it is stable. This is the concept of sample stability. As we show below, for a given parameter setting the Lyapunov exponent is for almost all trajectories, i.e., with Prob1, the same.

III. TRANSFER MATRIX FORMALISM

To illustrate the difficulties in treating the infinite product of random matrices of the above type we consider one of the standard methods, the transfer matrix formalism.

We denote the state $\vec{z}_{\sigma_{n+1}}(t_n+0)$ immediately after the jump from ε_{σ_n} to $\varepsilon_{\sigma_{n+1}}$ at time t_n by $\vec{z}_n$, the (random) time span between jumps $n-1$ and n by τ_n and write the recursion (2.9) as

$$\vec{z}_n=\mathbf{T}^{\sigma_n}(\tau_n)\vec{z}_{n-1}\equiv\mathbf{T}^{(n)}\vec{z}_{n-1}. \tag{3.1}$$

From Eq. (3.1) one obtains in the usual way closed second order recursion relations for q_n (or ψ_n). Introducing $R_{n+1}=q_{n+1}/q_n$ we arrive at

$$R_{n+1}=A_n+B_n\frac{1}{R_n}, \tag{3.2}$$

where

$$A_n=T_{11}^{(n+1)}+T_{12}^{(n+1)}\cdot T_{22}^{(n)}/T_{12}^{(n)}, \tag{3.3}$$

$$B_n=T_{12}^{(n+1)}(T_{21}^{(n)}+T_{22}^{(n)}\cdot T_{11}^{(n)}/T_{12}^{(n)}). \tag{3.4}$$

Since $\mathbf{T}^{(n+1)}$ depends on τ_{n+1}, and $\mathbf{T}^{(n)}$ depends on τ_n, both A_n and B_n depend on τ_{n+1} and τ_n. This is the origin of the twofold integration with respect to the distribution of times between two consecutive jumps $\rho(t)=\alpha e^{-\alpha t}$ in the Frobenius-Perron equation associated with Eq. (3.2)

$$\tilde{P}_{n+1}(R)=\int d\tau'\int d\tau\int dR'\rho(\tau')\rho(\tau)\tilde{P}_n(R')\times\delta\left[R-A(\tau,\tau')-B(\tau,\tau')\frac{1}{R'}\right]. \tag{3.5}$$

The Lyapunov exponent that governs the long time behavior of q is

$$\lambda_q=\lim_{N\to\infty}\frac{1}{N}\ln\frac{q_N}{q_0}=\lim_{N\to\infty}\frac{1}{N}\sum_{n=0}^{N-1}\ln R_n=\int dR\tilde{P}_s(R)\ln R, \tag{3.6}$$

where the last equality holds with Prob1 and $\tilde{P}_s(R)$ is the stationary solution of Eq. (3.5). However, to the best of our knowledge, Eq. (3.5) does not belong to the class of

Frobenius-Perron equations, which were amenable to explicit determination of their stationary solution.

IV. AN ALTERNATIVE APPROACH

In this section we exploit an alternative approach [14] based on a transformation from (q,ψ) to polar coordinates (r,φ), which circumvents the problem of solving the above Frobenius-Perron equation.

In polar coordinates the dynamic equations (1.1)–(1.2) read

$$\dot{r}=g(\varepsilon_t,\varphi)r, \tag{4.1}$$

$$\dot{\varphi}=h(\varepsilon_t,\varphi), \tag{4.2}$$

where

$$g(\varepsilon_t,\varphi)=-\cos^2\varphi-\zeta\varepsilon_t\sin 2\varphi-(\varepsilon_0^2+\varepsilon_t^2)\sin^2\varphi, \tag{4.3}$$

$$h(\varepsilon_t,\varphi)=\cos^2\varphi[\zeta\varepsilon_t(\tan^2\varphi-1)+(1-\varepsilon_0^2-\varepsilon_t^2)\tan\varphi]. \tag{4.4}$$

Equation (4.1) is linear in r and can be solved for a given trajectory of the driving process. This leads to the Lyapunov exponent

$$\lambda=\lim_{t\to\infty}\frac{1}{t}\int_0^t d\tau\, g(\varepsilon_\tau,\varphi)=\int_{\mathrm{supp}} d\varphi\sum_{\sigma=\pm}P_\sigma(\varphi)g(\varepsilon_\sigma,\varphi). \tag{4.5}$$

The second equality holds due to the multiplicative ergodic theorem of Oseledec [34] with Prob1. Clearly, if $\lambda<0$ the trivial solution $r=0$ of Eq. (4.1) is stable and otherwise unstable. $P_\sigma(\varphi)$ is the stationary solution of the Kolmogorov forward equation of the joint process (ε_t,φ) associated with Eq. (4.2)

$$\dot{P}_\sigma=\frac{d}{d\varphi}(h_\sigma P_\sigma)-\alpha(P_{-\sigma}-P_\sigma),\quad \sigma=\pm, \tag{4.6}$$

where h_σ is the shorthand for $h(\varepsilon_\sigma,\varphi)$. For the *nonrotational case* the solution of Eq. (4.6) can be found up to quadratures [14] and leads to

$$4\lambda=-\sum_{\sigma=\pm}\mathrm{Sp}\,\mathbf{C}^\sigma-\frac{\int_{\mathrm{supp}}d\varphi\,F(d/d\varphi)\ln|h_+/h_-|}{\int_{\mathrm{supp}}d\varphi\,F/h_+}, \tag{4.7}$$

where

$$F(\varphi,\varphi_0)=\exp\left[-\alpha\int_{\varphi_0}^{\varphi}d\varphi\left(\frac{1}{h_+}+\frac{1}{h_-}\right)\right],\quad \varphi_0\in\mathrm{supp}. \tag{4.8}$$

The degenerate case where $\mathbf{C}^+$ and $\mathbf{C}^-$ have an eigenvalue in common deserves special consideration.

For our problem, the quadratures in Eqs. (4.7) and (4.8) can be explicitly evaluated in terms of generalized hypergeometric functions. For the case of pure stochastic excitation ($\varepsilon_1\equiv 0$) this was done in [10]. Here, we evaluate Eq. (4.7) for the general case $\varepsilon_1\neq 0$.

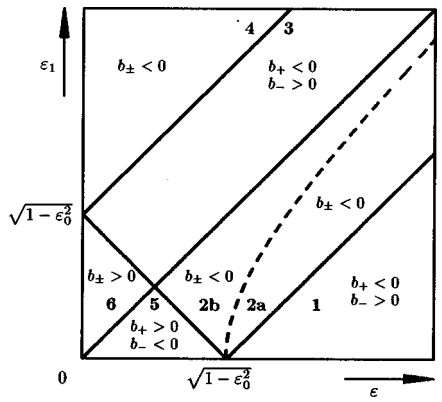

FIG. 1. Regions of the $\varepsilon-\varepsilon_1$ plane where b_+ and b_- do not change sign are separated by solid lines. The dashed line $\varepsilon_1^2=\varepsilon_0^2+\varepsilon^2-1$ separates 2a and 2b. The flow (4.9) is qualitatively different in region 6, regions 5 and 2b, and regions 2a and 1; cf. Fig. 2. Note that we used dimensionless quantities. The rescaling to physical units is given in Appendix B. Material parameters are taken from the set MBBA I.

A. Support

We determine the support of the process (4.2). The first step is to find the zeroes of the stochastic flow $h(\varepsilon_t,\varphi)$ for both realizations $h_\sigma(\varphi)$, $\sigma=\pm$. To this aim we write $h_\sigma(\varphi)$, introducing the shorthand $t=\tan\varphi$, as

$$\begin{aligned}h_\sigma(\varphi)&=\zeta\varepsilon_\sigma\cos^2\varphi(t^2+2b_\sigma t-1)\\&\equiv\zeta\varepsilon_\sigma\cos^2\varphi(t+Q_\sigma)\left(t-\frac{1}{Q_\sigma}\right),\end{aligned} \tag{4.9}$$

where

$$Q_\sigma=b_\sigma-\sqrt{b_\sigma^2+1},\quad b_\sigma=\frac{1-\varepsilon_0^2-\varepsilon_\sigma^2}{2\zeta\varepsilon_\sigma}. \tag{4.10}$$

The ε-ε_1 plane is divided into six regions where b_+ and b_- have a definite sign (see Fig. 1). The boundaries separating these regions are given by the zeroes of ε_- and b_σ. The following obviously hold: (i) sgn $\varepsilon_-=\pm$ for $\varepsilon_1\gtrless\varepsilon$; (ii) sgn $b_+=\pm$ for $1-\varepsilon_0^2-\varepsilon_{+<}^2\gtrless 0$, i.e., for $\varepsilon_1\gtrless-\varepsilon+\sqrt{1-\varepsilon_0^2}$; (iii) sgn $b_-=+$ for $1-\varepsilon_0^2-\varepsilon_{-<}^2\gtrless 0$ and $\varepsilon_{-<}\gtrless 0$, i.e., for $\varepsilon<\varepsilon_1<\varepsilon+\sqrt{1-\varepsilon_0^2}$ and $0<\varepsilon_1<\varepsilon-\sqrt{1-\varepsilon_0^2}$; sgn $b_-=-$ for $1-\varepsilon_0^2-\varepsilon_{-<}^2\gtrless 0$ and $\varepsilon_{->}\lessgtr 0$, i.e., for $\varepsilon+\sqrt{1-\varepsilon_0^2}<\varepsilon_1$ and $\varepsilon-\sqrt{1-\varepsilon_0^2}<\varepsilon_1<\varepsilon$.

To determine the sign of the flow $h_\sigma(\varphi)$ as a function of φ, cf. (4.9), we have to investigate the ordering of its zeroes

$$\varphi_{1\sigma}=\arctan(1/Q_\sigma), \tag{4.11}$$

$$\varphi_{2\sigma}=-\arctan Q_\sigma. \tag{4.12}$$

Since arctan is monotonic it is sufficient do discuss the ordering of $1/Q_\sigma$ and $-Q_\sigma$ ($\sigma=\pm$).

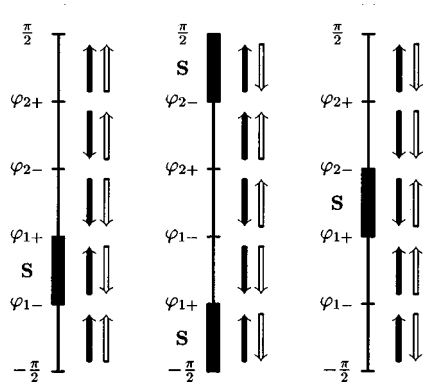

FIG. 2. Directions of the flow $h_\sigma(\varphi)$ for $\varphi\in[-\pi/2,\pi/2]$. The solid (open) arrows indicate the direction of the flow for the realization $\sigma=+$ $(-)$ of the driving process $\varepsilon_\sigma=\varepsilon_1+\sigma\varepsilon$. The regions with different directions of the flow are separated by $\varphi_{1\sigma}=\arctan(1/Q_\sigma)$ and $\varphi_{2\sigma}=-\arctan Q_\sigma$, $\sigma=\pm$. (a) shows the properties in region 6 of Fig. 1, (b) those of region 5 and 2b, (c) those of 2a and 1. The process, once trapped in the supporting interval S (marked by the fat bars), will never leave this interval since the flows in the neighborhood point toward S.

We first consider the regions 1 and 5 where b_+ and b_- have a different sign. Since $Q_+=Q_-$ is equivalent to $b_+=b_-$, which is in these regions never fulfilled there is a given order of Q_+ and Q_-, which holds in the entire region. In region 1 we have $b_+<0$ and $0<b_-$ which leads to $Q_+<Q_-<0$. In region 5 we have $b_-<0$ and $0<b_+$, which leads to $Q_-<Q_+<0$. In region 6 we have $0<b_+<b_-$. Observing that $1/Q_\sigma=-(b_\sigma+\sqrt{b_\sigma^2+1})<0$ this leads directly to $1/Q_-<1/Q_+<0$. In region 2 we have $b_+<0$ and $b_-<0$. It is obvious that $-Q_+>-Q_-$ for $-b_+>-b_-$. The latter inequality is equivalent to $\varepsilon_1^2<\varepsilon_0^2+\varepsilon^2-1$, which holds in region 2a. The same argument shows that $-Q_->-Q_+$ holds in 2b. Regions 3 and 4 are not considered here since the threshold curve—as it turns out—is outside of these regions.

We thus established in regions 1, 2a, and 6 of Fig. 1

$$\frac{1}{Q_-}\leqslant\frac{1}{Q_+}<0<-Q_-\leqslant-Q_+, \tag{4.13}$$

and in regions 2b and 5 of Fig. 1

$$\frac{1}{Q_+}\leqslant\frac{1}{Q_-}<0<-Q_+\leqslant-Q_-. \tag{4.14}$$

Now we discuss the example of region 6 in detail. The signs of the flow $h_\sigma(\varphi)$ shown in Fig. 2(a) depend only on the realization σ of the noise and on $\varphi\in[-\pi/2,\pi/2]$. For instance, we consider $\varphi\in[-\pi/2,\varphi_{1-}]$. In this interval $\mathrm{sgn}(t+Q_\sigma)=\mathrm{sgn}(t-1/Q_\sigma)$ is negative, and $\mathrm{sgn}\,\varepsilon_\sigma$ is positive. Therefore, the flow is positive for both realizations of the noise. Passing the boundary φ_{1-} of this interval the flow $h_-(\varphi)$ changes sign. Thus, in the interval $[\varphi_{1-},\varphi_{1+}]$ the flow changes sign when the process jumps between $+$ and $-$. Passing the next boundary φ_{1+}, the flow $h_+(\varphi)$ changes sign so that in $[\varphi_{1+},\varphi_{2-}]$ the flow is negative for both realizations of the noise. Obviously, the process, once trapped in

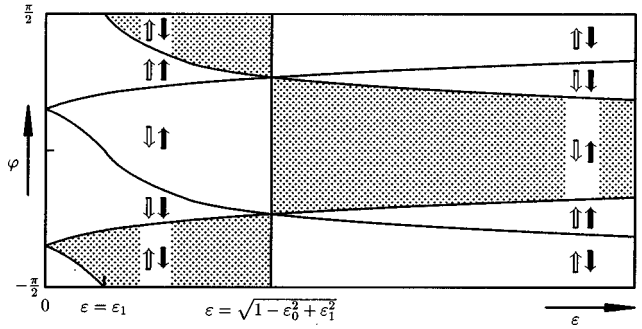

FIG. 3. Support S (dotted regions) as a function of ε for $\varepsilon_1\simeq0.27$. The directions of the flow h_σ are indicated by full and open arrows for $\sigma=-$ and $\sigma=+$, respectively. Note the periodicity with respect to $\varphi(\mathrm{mod}\,\pi)$. Material parameters are taken from the set MBBA I.

$$S=[\varphi_{1-},\varphi_{1+}], \tag{4.15}$$

will never leave this interval since the flows in the neighborhood point towards S. Therefore S and $S+\pi$, respectively, constitute the support of the stationary probability density $P_s(\varphi)=\Sigma_\sigma P_\sigma(\varphi)$.

In a similar way, the flows in the other regions are evaluated with the results shown in Figs. 2(b) and 2(c).

In regions 5 and 2b the support is given by

$$S=[-\pi/2,\varphi_{1+}]\cup[\varphi_{2-},\pi/2]. \tag{4.16}$$

In regions 2a and 1 the support is

$$S=[\varphi_{1+},\varphi_{2-}]. \tag{4.17}$$

Figure 3 shows for illustration the support as a function of ε for a special choice of ε_1, ζ, and ε_0.

B. Evaluation of integrals

Direct evaluation of Eq. (4.8) yields

$$F(\varphi,\varphi_0)=\frac{\tilde{F}(\tan\varphi)}{\tilde{F}(\tan\varphi_0)}, \tag{4.18}$$

where

$$\tilde{F}(t)=\prod_{\sigma=\pm}\left|\frac{t-1/Q_\sigma}{t+Q_\sigma}\right|^{\kappa_\sigma},\quad \kappa_\sigma=-\frac{\alpha}{\zeta\varepsilon_\sigma}\frac{1}{(Q_\sigma+1/Q_\sigma)}. \tag{4.19}$$

We remark that in Eq. (4.7) the factors $\tilde{F}(\tan\varphi_0)$ cancel so that we ignore these terms in the remainder. Equation (4.19) is needed to calculate the integrals that appear in Eq. (4.7). Both integrals in Eq. (4.7) can be reduced to integrals of the type

$$\tilde{I}(n,m_+,m_-)=\int_{\tan(S)}dt\;t^n\prod_\sigma\frac{|t-1/Q_\sigma|^{\kappa_\sigma}|t+Q_\sigma|^{-\kappa_\sigma}}{(t-1/Q_\sigma)^{m_\sigma}(t+Q_\sigma)^{m_\sigma}} \tag{4.20}$$

for $n=0,2$ and $m_\sigma=0,1$. The integral in the denominator of Eq. (4.7) is

$$\int_S d\varphi \frac{\tilde{F}}{h_+} = \frac{1}{\zeta\varepsilon_+}\int_{\tan(S)} dt \frac{\prod_\sigma |t-1/Q_\sigma|^{\kappa_\sigma}|t+Q_\sigma|^{-\kappa_\sigma}}{(t-1/Q_+)(t+Q_+)} = \frac{1}{\zeta\varepsilon_+}\tilde{I}(0,1,0). \tag{4.21}$$

Observing that

$$\frac{d}{d\varphi}\ln\left|\frac{h_+}{h_-}\right| = 2(b_- - b_+)\frac{(1+t^2)^2}{\prod_\sigma (t-1/Q_\sigma)(t+Q_\sigma)}, \tag{4.22}$$

we obtain the integral in the numerator of Eq. (4.7) as

$$\int_S d\varphi \tilde{F}\frac{d}{d\varphi}\ln\left|\frac{h_+}{h_-}\right| = 2(b_- - b_+)\int_{\tan(S)} dt(1+t^2) \times \prod_\sigma \frac{|t-1/Q_\sigma|^{\kappa_\sigma}|t+Q_\sigma|^{-\kappa_\sigma}}{(t-1/Q_\sigma)(t+Q_\sigma)} = 2(b_- - b_+)[\tilde{I}(0,1,1)+\tilde{I}(2,1,1)]. \tag{4.23}$$

With $b_- - b_+ = \varepsilon(1+\varepsilon_1^2-\varepsilon_0^2-\varepsilon^2)/(\zeta\varepsilon_+\varepsilon_-)$ the Lyapunov exponent is evaluated in terms of the integrals $\tilde{I}(n,m_+,m_-)$ as

$$-2\lambda = 1+\varepsilon_0^2+\varepsilon_1^2+\varepsilon^2 + \frac{\varepsilon(1+\varepsilon_1^2-\varepsilon_0^2-\varepsilon^2)}{\varepsilon_-}\frac{\tilde{I}(0,1,1)+\tilde{I}(2,1,1)}{\tilde{I}(0,1,0)}. \tag{4.24}$$

The *explicit* evaluation of the $\tilde{I}(n,m_+,m_-)$ in terms of generalized hypergeometric functions depends on the parameter region and is deferred to Appendix A.

C. The thresholds

The threshold corresponding to the criterion of the sample stability is obtained from the solution of Eq. (4.24) for $\lambda = 0$. For example, given ε, ε_0, and ζ, the solution $\varepsilon_1 = \varepsilon_{1\,\mathrm{th}}$ determines the threshold for the deterministic component of the driving field. Exploiting the analytical representation of $\tilde{I}(n,m_+,m_-)$ by generalized hypergeometric functions (cf. Appendix A) and its series representations [35–37] we solved Eq. (4.24) for $\lambda = 0$ numerically.

The results are compared with thresholds obtained from two different criteria (namely, the threshold of a simple mean-field decoupling and the threshold describing the stability of the first moments), and the threshold obtained by numerical simulations based on the *exact* formal solution (2.11).

We first describe a decoupling procedure [3], which assumes that the characteristic time of the driving stochastic process is fast compared to all characteristic times of the system. Then the system will ''feel'' only the average value of the stochastic field, which means $\varepsilon_t \to \langle\varepsilon_t\rangle = \varepsilon_1$ and $\varepsilon_t^2 \to \langle\varepsilon_t^2\rangle = \varepsilon_1^2+\varepsilon^2$ (This physical picture corresponds to a simple mean-field type decoupling $\langle\varepsilon_t\vec{z}\rangle \to \langle\varepsilon_t\rangle\langle\vec{z}\rangle$ of the averages). With the above replacements in Eq. (1.2) we obtain from $\det \mathbf{C} = 0$ the threshold

$$\varepsilon_{1,\mathrm{th}}^2 = \frac{\varepsilon_0^2+\varepsilon^2}{\zeta^2-1}. \tag{4.25}$$

The stability of the first (and higher) moments was extensively studied in [8–10] on the basis of *exact* equations of motions for $\langle\vec{z}\rangle$ and $\langle\varepsilon_t^{\mathrm{DMP}}\vec{z}\rangle$, which form a closed system due to the theorem of Shapiro and Loginov [38] $(\partial/\partial t + 2\alpha)\langle\varepsilon_t^{\mathrm{DMP}}\vec{z}\rangle = \langle\varepsilon_t^{DMP}\dot{\vec{z}}\rangle$. For $2\alpha > \zeta^2-1$ the threshold of the first moments is determined by a parabola in the $\varepsilon^2-\varepsilon_1^2$ plane [8,9]

$$(\varepsilon_1^2-\varepsilon^2)^2-(c_1+c_2)\varepsilon^2-(c_3+c_1c_2/c_3)\varepsilon_1^2+c_1c_2=0, \tag{4.26}$$

where $c_1 = (\varepsilon_0^2+2\alpha)/(\zeta^2-1)$, $c_2 = \varepsilon_0^2(1+2\alpha)/(\zeta^2-1-2\alpha)$, and $c_3 = \varepsilon_0^2/(\zeta^2-1)$.

For pure stochastic excitation the first moment's threshold is found in [8,9] as

$$\varepsilon_{\mathrm{th}}^2 = \begin{cases} \min(c_1,c_2) & \text{for } 2\alpha \leqslant \zeta^2-1. \\ c_1 & \text{for } 2\alpha \geqslant \zeta^2-1. \end{cases} \tag{4.27}$$

The numerical simulation investigates trajectories $\vec{z}(t)$ starting from a nonzero but small initial value $\vec{z}(0)$ for a given realization of the driving stochastic process $\varepsilon_t^{\mathrm{DMP}}$, i.e., for a given sequence of jumping times $t_1, \ldots, t_n$. A trajectory with N jumps (corresponding to a typical time N/α) is considered as exploding if $\psi = \partial_x\varphi \sim k\varphi = (\pi\varphi)/d > \pi^2/(4d)$, i.e., for $\varphi > \varphi_c \approx \pi/4$. This critical value for φ is chosen, because for $\varphi \gtrsim \pi/4$ the linearization of $\sin\varphi \approx \varphi$, which leads to our initial linear differential equation, is certainly wrong. We have checked that the thus determined thresholds are practically independent of N and ψ_c for $N \gtrsim 10^4$ (i.e., vary only within a margin of less than 1%) by varying both N and ψ_c over a range of several orders of magnitude.

Figures 4 and 5 show the thresholds according to the above criteria for pure stochastic excitation and for the superposition of a constant with a stochastic voltage. (For the change from dimensionless quantities to physical units consult Appendix B.) The numerical simulations strongly confirm the results obtained from the criterion of sample stability. The region describing the stability of the moments is always smaller than the region of sample stability but shows qualitatively a similar behavior.

We remark that for identical parameters and wave numbers the threshold for stochastic excitation (irrespective of the criteria) is always below that for deterministic excitation. This is understandable since a stochastic trajectory with a given mean number of jumps always contains slower Fourier components, which lead to a lower threshold. In the static

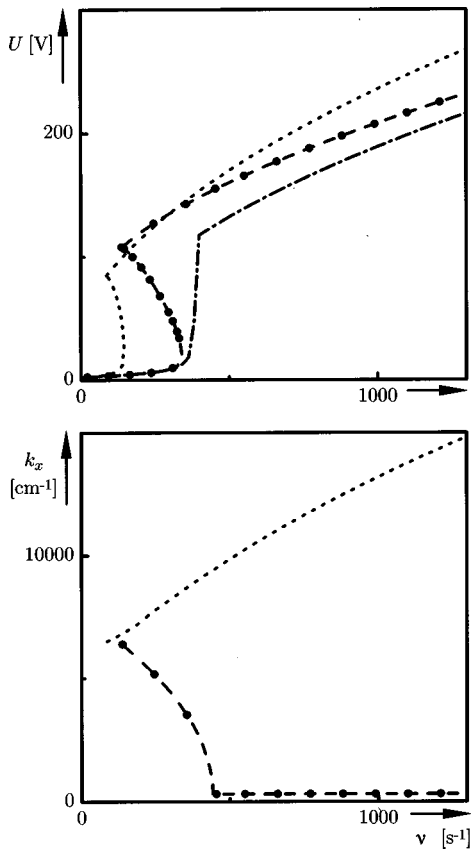

FIG. 4. Stability of the undistorted state against the appearance of rolls for the one-dimensional model. Shown are thresholds as a function of the (mean) number of jumps for excitation by a deterministic square voltage (dotted line) and by a dichotomous stochastic voltage. In the stochastic case the thresholds are obtained from stability of first moments (dash-dotted line), from sample stability (dashed line), and from numerical simulation (•) of a stochastic trajectory of about 10^5 jumps based on the formal solution (2.11); the errors are within the thickness of the line. The lower part of the figure shows the selected wave number for the *dielectric* mode; we chose π/d as a lower cutoff for k_x. (The threshold of the first moments decreases monotonically with k_x so that there is no mode selection.) Material parameters correspond to MBBA II.

limit $\alpha \to 0$ only the sample stability threshold converges to the deterministic result; the threshold of the moments reproduces only the lower branch.

In Fig. 5 we note that for small values of the stochastic voltage U all thresholds coincide as expected. For a large range of U the threshold from mean field decoupling is very near to that of sample stability but for U beyond the threshold for pure stochastic excitation ($U_1=0$) both thresholds are drastically different. This behavior can be understood by comparing the characteristic times of the system and of the noise.

The characteristic times of the full (stochastically driven) system are by modulus the inverse of the Lyapunov exponents $\lambda_2<\lambda_1$ of the system. At the threshold we have $\lambda_1=0$, the corresponding characteristic time diverges and is thus well separated from τ_{stoch}. Since $\lambda_1+\lambda_2=1/2\Sigma_\sigma \mathrm{Sp}\mathbf{C}^\sigma$ [14] we can evaluate the second characteristic time at the threshold

$$\tau_2=|1/\lambda_2|=(1+\varepsilon_0^2+\varepsilon^2+\varepsilon_1^2)^{-1}. \tag{4.28}$$

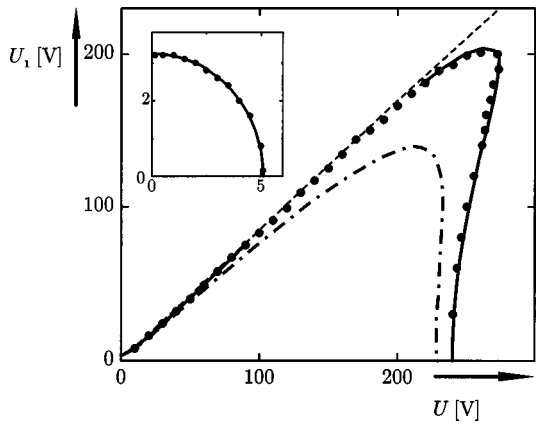

FIG. 5. Stability of the one-dimensional model against the appearance of roll cells in the case of a superposition of constant voltage U_1 and stochastic dichotomous voltage U for a ''fast'' driving field ($\nu \simeq 1000$ s^{-1}). The thresholds are obtained from (i) a simple mean-field decoupling (dashed line), (ii) stability of first moments (dash-dotted line), and (iii) sample stability (solid line). The numerical simulation threshold is indicated by (•). Note that we refrained from evaluating the analytic threshold condition for sample stability in the range (90 V, 75 V)$<(U,U_1)<$(216 V,180 V) which leads to generalized hypergeometric functions of $n \geqslant 4$ arguments because of the excellent agreement with the simulation in the other regions. Material parameters are taken from the set MBBA I. The insert shows the case of a ''slow'' driving field for which the three criteria give the same threshold ($\nu \simeq 100$ s^{-1}, $\sigma_\parallel = 1.5\times10^{-10}\Omega^{-1}$ cm^{-1}, $\sigma_\parallel/\sigma_\perp = 1.3$, other material parameters from MBBA I).

With increasing values of the fields at the threshold τ_2 decreases and may reach the order of τ_{stoch} (which is small but nonzero) as illustrated in Fig. 6. In the latter case, the mean-field-like decoupling is not justified and the corresponding threshold is manifestly wrong, cf. Fig. 5.

The exact treatment of the moments takes the finite characteristic time τ_{stoch} of the driving process properly into account. Therefore, one finds a finite threshold for pure sto-

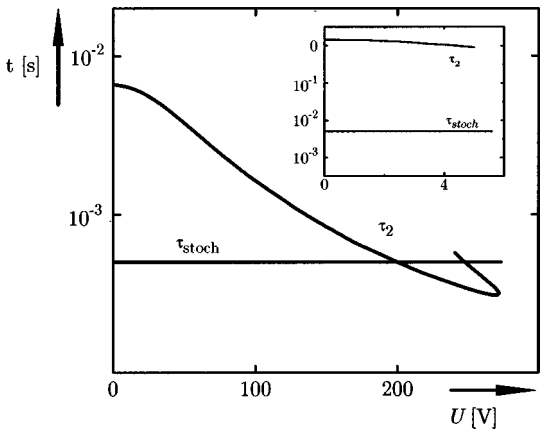

FIG. 6. The characteristic time $\tau_2=|1/\lambda_2|$ at the sample stability threshold shown in Fig. 5 decreases with increasing voltage. The initially clearly separated time scales of τ_2 and $\tau_{\text{stoch}}=1/2\nu$ become of the same order at sufficiently high stochastic voltage. The inset shows that for the ''slow'' driving case the time scales are well separated.

chastic excitation. The region of stable moments is always smaller than that for sample stability but possibly of similar shape. The former is obvious [10] since the divergence of the trajectories is sufficient for the divergence of the moments: For large times we have $r_t = e^{\langle \lambda[\varepsilon_\tau]\rangle t} \leqslant \langle e^{\lambda[\varepsilon_\tau]t}\rangle = \langle r_t\rangle$ where the inequality holds due to the convexity of the exp function.

The superposition of a deterministic field with a ''fast'' stochastic field may lead to a region of sample stability that extends beyond the threshold values of deterministic or stochastic driving alone, thus forming a stable tongue in the $U-U_1$ plane. This explains naturally why in experiments [4–7], applying first a stochastic voltage U of a given strength and increasing then the deterministic voltage U_1 up to the instability of the homogeneous phase, a discontinuous behavior of the thus determined threshold was observed: Below U_c the threshold of the deterministic voltage $U_{1\mathrm{th}}$ appears finite and above zero. A similar behavior (but less pronounced) was observed previously [8–10] considering the stability of moments, cf. also Fig. 5.

We further remark that the moment's stability may be totally misleading if characteristic times of noise and system are of comparable order in a larger parameter range. For example, we found for a noise of mean number of jumps $\alpha = 0.66$ (parameter setting MBBA I as given in Appendix B) a very pronounced stable tongue for sample stability but for the stability of the moments we found a monotonic decreasing threshold. If instead τ_{stoch} is clearly separated from at least one characteristic time of the system, both moment's and sample stability criteria give similar results (see insets in Figs. 5 and 6).

The appearance of a stable tongue depends also on the material parameters. Roughly speaking, the tendency towards formation of a stable tongue decreases with increasing Helfrich parameter ζ^2 as observed already in [8] using moment's stability. This is confirmed also for sample stability thresholds, comparing results for the two sets of material parameters MBBA I and MBBA II given in Appendix B, which correspond to $\zeta^2 = 2.39$ and $\zeta^2 = 3.08$, respectively (see Table I). (The lower value is just above the critical value 2.35 below which there is for the one-dimensional model no mode selection in the deterministic high frequency limit [29].)

A further important parameter is the conductivity, which may, however, differ from sample to sample considerably and which can be changed easily by doping. The ratio $\sigma_\parallel/\sigma_\perp$, which alone enters the Helfrich parameter, is a more stable characteristics. The parallel component of the conductivity $\sigma_\parallel$ comes into play if we return from the dimensionless variables of the one-dimensional theory to variables in physical units, see Appendix B, Eqs. (B2) and (B3). Roughly speaking, the tendency towards formation of a stable tongue increases with increasing $\sigma_\parallel$ while $\sigma_\parallel/\sigma_\perp$ is kept constant (cf. Fig. 7).

We remark that the early experiments [4–7] were performed with highly salted MBBA [39]; no characterization of the material was given. In later experiments [40,41] with unsalted MBBA and a different chemically more stable nematics (for both ζ^2 was in the range 3–4) no stable tongue and correspondingly no discontinuous behavior of the threshold was found.

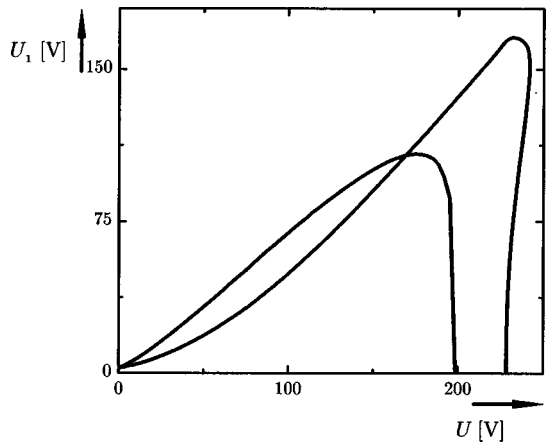

FIG. 7. Comparison of sample stability thresholds for different values of the conductivity in the one-dimensional model. The tendency towards formation of a stable tongue increases with increasing conductivity. Shown are the cases $\sigma_\parallel = 0.75\times10^{-10}\ \Omega^{-1}\ \mathrm{cm}^{-1}$ and $\sigma_\parallel = 3\times10^{-10}\ \Omega^{-1}\ \mathrm{cm}^{-1}$, $\sigma_\parallel/\sigma_\perp = 1.5$. In the latter case there is a stable tongue so that, following the measuring procedure described in the text, the threshold curve appears discontinuous. The mean number of jumps is $\nu = 1000\ \mathrm{s}^{-1}$, other parameters are taken from MBBA II.

V. TWO-DIMENSIONAL MODEL

In the two-dimensional version the equations describing the stability of the undistorted state against formation of rolls are similar to the one-dimensional case. It is more convenient now to use variables in physical units denoted by $\tilde{q}$ and $\tilde{\psi}$. The dynamics of $\vec{z} = (\tilde{q}, \tilde{\psi})^T$ is given by Eq. (1.1), where now

$$\mathbf{C}(t) = -\begin{pmatrix} 1/T_q & \sigma_H E_t \\ a E_t & \Lambda_1 - \Lambda_2 E_t^2 \end{pmatrix}. \tag{5.1}$$

The coefficients $1/T_q$, σ_H, a, Λ_1, and Λ_2 given in Appendix C depend all on the wave numbers k_x and k_z to be determined by mode selection. $E_t = E_1 + E_t^{\mathrm{DMP}}$ is the superposition of a constant field E_1 and a dichotomous stochastic field E_t^{DMP} with the same statistical properties as $\varepsilon_t^{\mathrm{DMP}}$. E_t takes the values $E_\sigma = E_1 + \sigma E$, $\sigma = \pm$. Introducing polar coordinates as in Sec. IV the analog to Eq. (4.9) reads

$$h_\sigma(\varphi) = \sigma_H E_\sigma \cos^2\varphi (t - Q_\sigma^1)(t - Q_\sigma^2), \tag{5.2}$$

where

$$Q_\sigma^{1/2} = -B_\sigma \pm \sqrt{B_\sigma^2 + \frac{a}{\sigma_H}}, \quad B_\sigma = \frac{1/T_q - \Lambda_1 + \Lambda_2 E_\sigma^2}{2\sigma_H E_\sigma}. \tag{5.3}$$

The formal result (4.7), (4.8) for the Lyapunov exponent holds also in this case; the analog to Eq. (4.19) is

$$\tilde{F}(t) = \prod_{\sigma=\pm} \left| \frac{t - Q_\sigma^2}{t - Q_\sigma^1} \right|^{\kappa_\sigma}, \quad \kappa_\sigma = \frac{\alpha}{\sigma_H E_\sigma} \frac{1}{(Q_\sigma^1 - Q_\sigma^2)}. \tag{5.4}$$

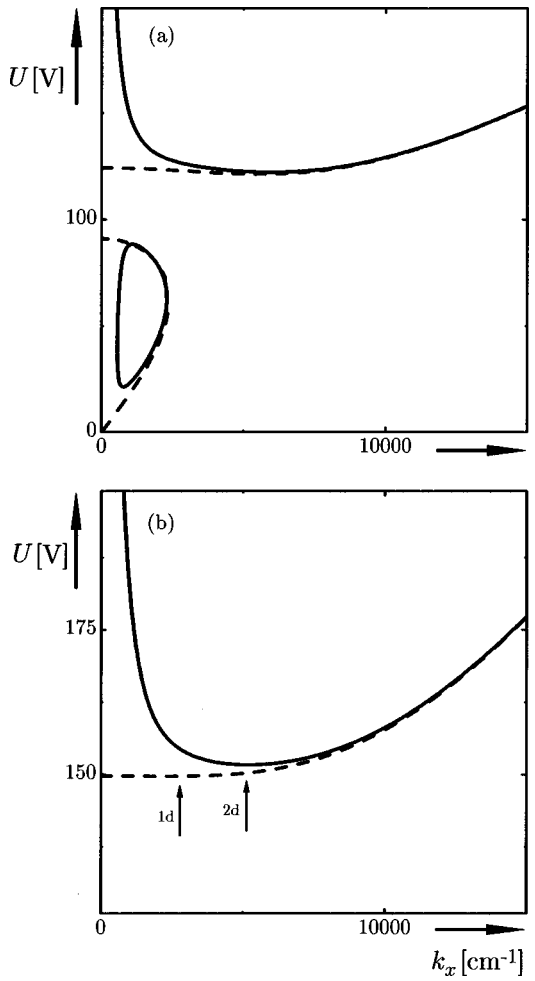

FIG. 8. Mode selection for pure stochastic excitation. Shown are the neutral curves for the one-dimensional model (dashed line) and the two-dimensional model (solid line) in (a) the conductive regime ($\nu = 100$ s^{-1}) and in (b) the dielectric regime ($\nu = 400$ s^{-1}). The unstable region in the left lower corner of (a) corresponding to the conductive mode shrinks with increasing mean frequency of the driving process and is absent in the dielectric regime (b). This topological difference explains the sharp crossover frequency in Figs. 4 and 9. We further see in (a) that for the one-dimensional model (dashed line) the absolute minimum of the neutral curve is at $k_x = 0$ so that mode selection fails. The arrows in (b) indicate the selected wave numbers for one- and two-dimensional models, which may differ considerably whereas the corresponding threshold voltages almost coincide; cf. Fig. 9. (The minimum of the dashed curve becomes more pronounced with increasing Helfrich parameter but it remains very flat for a reasonable range of ζ^2.) Material parameters are taken from the set MBBA II.

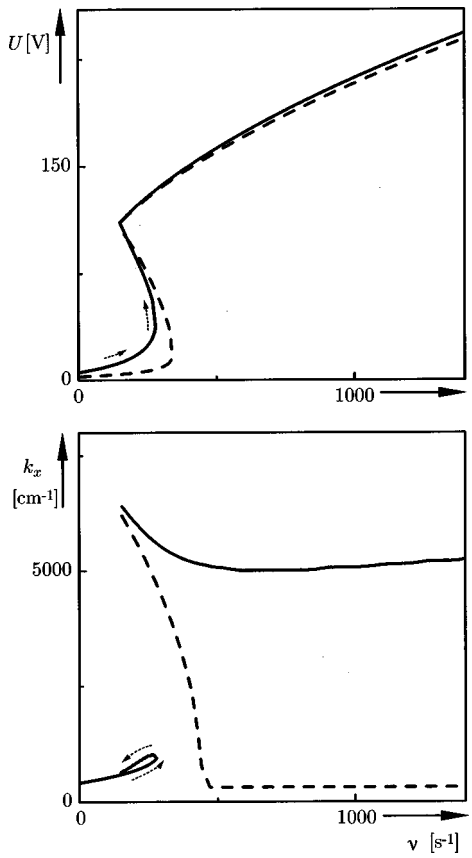

FIG. 9. Comparison of sample stability thresholds and selected wave numbers in the case of pure stochastic exitation for the one-dimensional (dashed line) and two-dimensional version (solid line). In the latter case, mode selection works also for the conductive mode. Note that the selected wave numbers differ considerably in the dielectric regime, which has, however, little influence on the thresholds. Material parameters are taken from the set MBBA II.

The further calculations, as, for instance, the determination of the support and the explicit evaluation of the integrals in (4.7),(4.8), are even more cumbersome than in the one-dimensional case, should be repeated several times in the process of mode selection, and are therefore done numerically. We always found $k_z = \pi/d$. In all considered cases the results of numerical evaluation of the Lyapunov exponent show a fair agreement with digital simulations, for not too large strength of the stochastic field within the thickness of the lines.

In Figs. 8–10 we compare the results for the one- and two-dimensional versions for pure stochastic excitation and for the superposition of a constant field with a stochastic field. The thresholds show qualitatively the same behavior, the quantitave difference is marginal. The selected wave numbers, however, show significant differences.

The stability chart for pure stochastic excitation (cf. Fig. 8) shows a topological difference between ''slow'' and ''fast'' driving. In the former case we have an unstable island in the left lower corner of Fig. 8(a). The corresponding mode (low threshold and small wave number) is called conductive. With increasing mean frequency of the driving field this island shrinks. There is a sharp transition if it disappears: The instability is now towards a mode with a higher threshold and a larger wave number, as is typical for the dielectric regime [cf. Fig. 8(b)]. We remark that also for deterministic driving the stability chart has these properties. The change of topology is not bound to the different symmetries of the dielectric and conductive mode, which is known to be restricted to deterministic driving.

In the conductive regime mode selection leads in the one-dimensional model to the unphysical value $k_x = 0$, which is as usual replaced by π/d. The *selected* wave number of the two-dimensional model is of the order π/d.

In the dielectric regime the selected wave number of the one-dimensional model decreases monotonically with in-

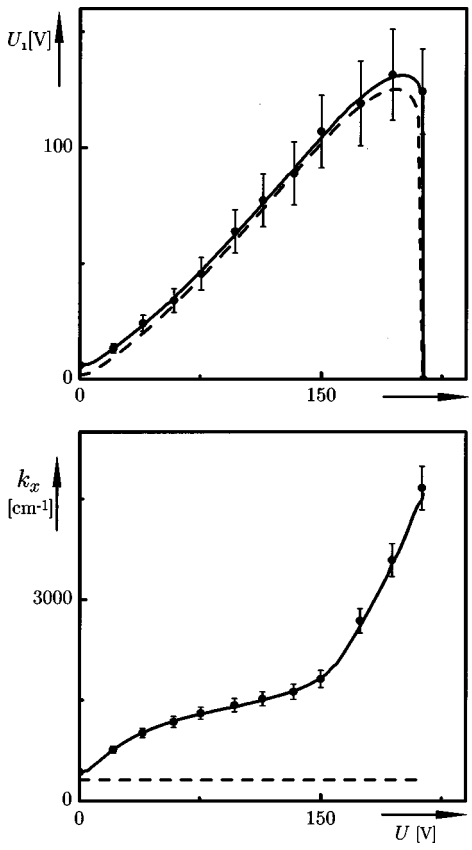

FIG. 10. Comparison of thresholds and selected wave numbers for the superposition of a constant with a stochastic dichotomous voltage obtained from the sample stability criterion for the one-dimensional model (dashed line) and the two-dimensional model (solid line). Material parameters are taken from MBBA II, $\nu = 1000\ \mathrm{s}^{-1}$.

creasing mean frequency and reaches rapidly the cutoff value π/d (cf. Fig. 9). The two-dimensional version shows more realistic behavior. With increasing mean frequency the wave number decreases first and then increases with a slope much smaller than for deterministic driving as is qualitatively also found in experiment [42].

For the superposition of deterministic and stochastic field (cf. Fig. 10) the wave number for the one-dimensional version is given by the cutoff value whereas for the two-dimensional version it increases drastically with increasing strength of the stochastic field, which qualitatively corresponds better to experimental findings [40–42]. A detailed quantitative comparison of two-dimensional theory and experiment is in preparation.

VI. CONCLUDING REMARKS

In studying a linearized version of the electrohydrodynamic equations we tacitly assumed that the system undergoes a supercritical bifurcation. It could, however, not be excluded that there is a noise-induced change from supercritical to subcritical bifurcation as found in different models [43–45]. For electrohydrodynamic convection in liquid crystals there are only vague experimental hints of noise induced hysteresis.

A theoretical treatment of the full set of nonlinear electrohydrodynamic equations seems at present not feasible. For deterministic systems, a weakly nonlinear analysis leads to simpler (but still complicated enough) amplitude equations [46]. In the stochastic case, see e.g., [47–51] it seems *a priori* not clear whether this approach would lead to equations with stochastic or averaged coefficients, having in mind that for our system the time scales are not always well separated and that it was crucial to take the finite correlation time of the noise properly into account.

Nonlinear partial differential equations, e.g., of Ginzburg-Landau or Swift-Hohenberg type, with *ad hoc* assumed additive or multiplicative Gaussian white noise are at present a subject of intense study, both numerically and analytically [52–65]. In this context in a spirit very close to ours, Becker and Kramer [64,65] found a controlable approximation to determine the threshold of sample stability without knowledge of the stationary distribution. A zero-dimensional version, the Stratonovich model, was solved rigorously for Gaussian white noise [66] and dichotomous noise [67].

In both the one- and two-dimensional versions of the standard model considered here the conductivity enters as a material parameter. Recently, Treiber and Kramer [68] developed a more sophisticated model where ionic migration, diffusion, and dissociation-recombination are included so that the conductivity becomes a variable that introduces new time and length scales. The analysis of stochastic driving within this model remains a task for the future.

In this paper we considered the stability of the undistorted state against *one* mode describing rolls of a given wave number. We expect, however, that, if the characteristic time of the noise is of the order of the inverse growing rate of a typical mode, the process of mode selection will be not completed until the next jump of the noise, so that a band of wave numbers is involved. This could lead to a sort of dynamical pattern as observed in experiment.

We observed in the digital simulations of the two-dimensional model that the fluctuations in the distribution of Lyapunov exponents for trajectories of finite length (which mean fluctuations of the threshold) increase if the characteristic times of noise and system become comparable, cf. Fig. 10. The analytic treatment of these fluctuations leads to the problem of generalized Lyapunov exponents [26,69]. Fluctuations of thresholds were also observed in experiment for large enough noise [40–42].

Finally we remark that it would be interesting to look for different physical systems described by infinite products of random matrices of the type considered here.

ACKNOWLEDGMENTS

Thanks are due to Lorenz Kramer for making Refs. [64,65] available to us prior to publication. The authors acknowledge support from the Deutsche Forschungsgemeinschaft DFG under Grant No. Be1417/3. One of us (A.L.) is grateful to the Deutsche Akademische Austauschdienst (DAAD) for financial support.

APPENDIX A

The evaluation of the integral $\tilde{I}$ given by Eq. (4.20) in terms of generalized hypergeometric functions depends on

the parameter region. In any case, we arrive at integrals of the form

$$I(\alpha,\beta_1,\beta_2,\gamma;x_1,x_2)=\int_0^1 du\, u^{\alpha-1}(1-u)^{\gamma-\alpha-1}\times(1+x_1u)^{-\beta_1}(1-x_2u)^{-\beta_2}, \tag{A1}$$

where $|x_2|<1$ but $|x_1|$ is not generally bounded by 1. Only if $|x_1|<1$ the integral (A1) is *immediately* related to the generalized hypergeometric function of *two* arguments, cf. the general definition [35–37],

$$F_D(\alpha,\beta_1,\ldots,\beta_n,\gamma;x_1,\ldots,x_n)=\frac{\Gamma(\gamma)}{\Gamma(\alpha)\Gamma(\gamma-\alpha)}\int_0^1 du\, u^{\alpha-1}(1-u)^{\gamma-\alpha-1}\times(1-x_1u)^{-\beta_1}\cdots(1-x_nu)^{-\beta_n}, \tag{A2}$$

where $|x_i|<1$, $i=1,\ldots,n$.

We consider the case $1<x_1<2$, which leads to a representation by generalized hypergeometric functions of *three* arguments. Choosing an arbitrary X, $x_1<X<2$, the transformation $Xu=v$ yields

$$I=X^{-\alpha}\int_0^X dv\, v^{\alpha-1}\left(1-\frac{1}{X}v\right)^{\gamma-\alpha-1}\left(1+\frac{x_1}{X}v\right)^{-\beta_1}\times\left(1-\frac{x_2}{X}v\right)^{-\beta_2}. \tag{A3}$$

We now split the integral in Eq. (A3) into two parts, $X^{-\alpha}(\int_0^1 dv+\cdots+\int_0^X dv\cdots)=I_1+I_2$, with obvious meaning of $I_{1/2}$. I_1 is already of normal form, i.e., directly related to F_D. The second integral I_2 is subject to the transformation $z=(v-1)/(X-1)$, which leads to

$$I_2=X^{-\alpha}(X-1)\left(1-\frac{1}{X}\right)^{\gamma-\alpha-1}\left(1+\frac{x_1}{X}\right)^{-\beta_1}\times\left(1-\frac{x_2}{X}\right)^{-\beta_2}\int_0^1 dz[1+(X-1)z]^{\alpha-1}(1-z)^{\gamma-\alpha-1}\times\left(1+\frac{X-1}{X+x_1}x_1z\right)^{-\beta_1}\left(1-\frac{X-1}{X-x_2}x_2z\right)^{-\beta_2}. \tag{A4}$$

Since $1<x_1<X<2$ the modulus of all coefficients of z is smaller than one and we arrive at

$$\begin{aligned}I(\alpha,\beta_1,\beta_2,\gamma;x_1.x_2)&=\frac{1}{\alpha X^{\alpha}}F_D\left(\alpha,1+\alpha-\gamma,\beta_1,\beta_2,\alpha+1;\frac{1}{X},-\frac{x_1}{X},\frac{x_2}{X}\right)\\&+\frac{X-1}{(\gamma-\alpha)X^{\alpha}}\left(1-\frac{1}{X}\right)^{\gamma-\alpha-1}\left(1+\frac{x_1}{X}\right)^{-\beta_1}\left(1-\frac{x_2}{X}\right)^{-\beta_2}\\&\times F_D\left(1,\beta_1,\beta_2,1-\alpha,\gamma-\alpha+1;-\frac{X-1}{X+x_1}x_1,\frac{X-1}{X-x_2},1-X\right).\end{aligned} \tag{A5}$$

The cases $n<x_1<n+1$, $n=2,3,\ldots$, can be treated by repeating this procedure $n-1$ times, which leads to generalized hypergeometric functions of $n+2$ arguments. We refrained, however, from extending the numerical calculations to $n\geqslant 2$.

We now evaluate $\tilde{I}$ in the different parameter regions in consecutive order.

1. In regions 1 and 2a the support is $S=[\varphi_{1+},\varphi_{2-}]$; cf. Eq. (4.17). From Eqs. (4.11),(4.12) we get $\tan(S)=[1/Q_+,-Q_-]$. For $t\in\tan(S)$ we have $t-1/Q_\sigma>0$ and $t-(-Q_\sigma)<0$; cf. Fig. 2(c), so that Eq. (4.20) can be written as

$$\tilde{I}(n,m_+,m_-)=(-1)\sum_\sigma{}^{m_\sigma}\int_{1/Q_+}^{-Q_-}dt\,t^n\prod_{\sigma=\pm}\left(t-\frac{1}{Q_\sigma}\right)^{\kappa_\sigma-m_\sigma}\times(-t-Q_\sigma)^{-\kappa_\sigma-m_\sigma}. \tag{A6}$$

Introducing the shorthands

$$l=1/Q_+-1/Q_-,\qquad s=-Q_--1/Q_+,\qquad r=-Q_+-(-Q_-), \tag{A7}$$

where obviously $l,s,r\geqslant 0$, the transformation $t'=(t-1/Q_+)/s$ yields

$$\tilde{I}(n,m_+,m_-)=(-1)\sum_\sigma{}^{m_\sigma}s^{1+\kappa_+-m_+-\kappa_--m_-}l^{\kappa_--m_-}\times(s+r)^{-\kappa_+-m_+}\int_0^1 dt'\left(st'+\frac{1}{Q_+}\right)^n\times t'^{\kappa_+-m_+}(1-t')^{-\kappa_--m_-}\times\left(1+\frac{s}{l}t'\right)^{\kappa_--m_-}\left(1-\frac{s}{s+r}t'\right)^{-\kappa_+-m_+}. \tag{A8}$$

In our case, cf. Eq. (4.24), n is an integer so that the integral in Eq. (A8) leads to integrals of the form (A1).

Only for $0<s/l<1$ is Eq. (A8) immediately related to the generalized hypergeometric function of two arguments. For $s/l>1$ and as long as $0<s/(s+r)<0.5$ holds, we exploit two *types* of transformations for F_D[see [36], p. 116, Eqs. (10_3) and (10_{n+3})], which finally give the transformation $t'=1-z$ for the integral in Eq. (A8). We obtain, introducing

$$\mathcal{I}_1=I\left(1-\kappa_-,-\kappa_-,\kappa_++1,\kappa_++1-\kappa_-;-\frac{s}{s+l},-\frac{s}{r}\right), \tag{A9}$$

$$\mathcal{I}_2=I\left(-\kappa_-,-\kappa_-+1,\kappa_++1,\kappa_+-\kappa_-;-\frac{s}{s+l},-\frac{s}{r}\right), \tag{A10}$$

$$\mathcal{I}_3=I\left(-\kappa_-,-\kappa_-+1,\kappa_++1,\kappa_++1-\kappa_-;-\frac{s}{s+l},-\frac{s}{r}\right), \tag{A11}$$

$$\mathcal{I}_4=I\left(-\kappa_-,-\kappa_-+1,\kappa_++1,\kappa_++2-\kappa_-;-\frac{s}{s+l},-\frac{s}{r}\right), \tag{A12}$$

the integrals appearing in Eq. (4.24) as

$$\tilde{I}(0,1,0) = -\xi(ls+s^2)\mathcal{I}_1, \tag{A13}$$

$$\tilde{I}(0,1,1) = \xi\mathcal{I}_2, \tag{A14}$$

$$\tilde{I}(2,1,1) = \xi\left[\frac{1}{Q_+^2}\mathcal{I}_2 + \frac{2s}{Q_+}\mathcal{I}_3 + s^2\mathcal{I}_4\right], \tag{A15}$$

where the factors $\xi = s^{\kappa_+-\kappa_--1}l^{\kappa_--1}(s+r)^{-\kappa_+-1}(1+s/l)^{\kappa_-}[1-s/(s+r)]^{-\kappa_+-1}$ cancel in Eq. (4.24). Since $s/r<1$ for $0<s/(s+r)<0.5$ and $s/(s+l)<1$, the integrals $\mathcal{I}_1,\ldots,\mathcal{I}_4$ are directly related to hypergeometric functions of *two* arguments.

2. In the regions 2b and 5 we obtain from Eqs. (4.11), (4.12), and (4.16) $\tan(S)=[-\infty,1/Q_+]\cup[-Q_-,\infty]$. Observing the signs of $t-1/Q_\sigma$ and $t+Q_\sigma$ in both intervals we can write

$$\begin{aligned}\tilde{I}(n,m_+,m_-) = &\int_{-\infty}^{1/Q_+} dt\, t^n \prod_\sigma \left(\frac{1}{Q_\sigma}-t\right)^{\kappa_\sigma-m_\sigma} \\ &\times(-Q_\sigma-t)^{-\kappa_\sigma-m_\sigma} + \int_{-Q_-}^{\infty} dt\, t^n \\ &\times\prod_\sigma \left(t-\frac{1}{Q_\sigma}\right)^{\kappa_\sigma-m_\sigma}(t+Q_\sigma)^{-\kappa_\sigma-m_\sigma}.\end{aligned} \tag{A16}$$

Introducing the shorthands [in contrast to Eqs. (A7)] we have

$$\begin{aligned} l &= Q_+ - Q_-, \\ s &= -1/Q_- - Q_+, \\ r &= -1/Q_+ + 1/Q_-, \end{aligned} \tag{A17}$$

which are obviously non-negative, the transformation $t' = (1/t - Q_+)/s$ leads to

$$\begin{aligned}\tilde{I}(n,m_+,m_-) = s&\left(1-\frac{Q_+}{Q_-}\right)^{\kappa_--m_-}\left(\frac{-s}{Q_+}\right)^{\kappa_+-m_+} \\ &\times(1+Q_+^2)^{-\kappa_+-m_+}(1+Q_-Q_+)^{-\kappa_--m_-} \\ &\times\int_0^1 dt'\, t'^{\kappa_+-m_+}(st'+Q_+)^{-2-n+2\sum_\sigma m_\sigma} \\ &\times\left(1+\frac{s}{l}t'\right)^{\kappa_--m_-}\left(1-\frac{s}{s+r}t'\right)^{-\kappa_+-m_+} \\ &\times(1-t')^{-\kappa_--m_-}.\end{aligned} \tag{A18}$$

Again, only for $0<s/l<1$ is Eq. (A18) immediately related to generalized hypergeometric functions of two arguments. For $1<s/l<2$ we follow the line described above. Introducing

$$\mathcal{I}_5 = I\left(\kappa_+,-\kappa_-,\kappa_++1,\kappa_++1-\kappa_-;\frac{s}{l},\frac{s}{s+r}\right), \tag{A19}$$

TABLE I. Material parameters of MBBA.

Quantitiy	MBBA I	MBBA II
$\varepsilon_\parallel$	4.5	4.72
$\varepsilon_\perp$	5.0	5.25
$\sigma_\parallel$ [Ω^{-1} cm^{-1}]	6.0×10^{-11}	1.5×10^{-10}
$\sigma_\perp$ [Ω^{-1} cm^{-1}]	4.6×10^{-11}	1.0×10^{-10}
α_1 [g cm^{-1} s^{-1}]		6.5×10^{-2}
α_4 [g cm^{-1} s^{-1}]	83.2×10^{-2}	83.2×10^{-2}
γ_1 [g cm^{-1} s^{-1}]	76.3×10^{-2}	76.3×10^{-2}
γ_2 [g cm^{-1} s^{-1}]	-78.7×10^{-2}	-78.8×10^{-2}
β [g cm^{-1} s^{-1}]	11.9×10^{-2}	11.9×10^{-2}
η_1 [g cm^{-1} s^{-1}]	103.5×10^{-2}	103.5×10^{-2}
η_2 [g cm^{-1} s^{-1}]	23.8×10^{-2}	23.8×10^{-2}
K_{11} [g cm s^{-2}]	6.1×10^{-7}	6.1×10^{-7}
K_{33} [g cm s^{-2}]	7.3×10^{-7}	7.25×10^{-7}
ζ^2	2.39	3.08

$$\mathcal{I}_6 = I\left(\kappa_+,-\kappa_-+1,\kappa_++1,\kappa_+-\kappa_-;\frac{s}{l},\frac{s}{s+r}\right), \tag{A20}$$

$$\mathcal{I}_7 = I\left(\kappa_++1,-\kappa_-+1,\kappa_++1,\kappa_++1-\kappa_-;\frac{s}{l},\frac{s}{s+r}\right), \tag{A21}$$

$$\mathcal{I}_8 = I\left(\kappa_++2,-\kappa_-+1,\kappa_++1,\kappa_++2-\kappa_-;\frac{s}{l},\frac{s}{s+r}\right), \tag{A22}$$

the integrals in Eq. (4.24) are then

$$\begin{aligned}\tilde{I}(0,1,0) &= \xi' ls\mathcal{I}_5, \\ \tilde{I}(0,1,1) &= \xi'(Q_+^2\mathcal{I}_6 + 2sQ_+\mathcal{I}_7 + s^2\mathcal{I}_8), \\ \tilde{I}(2,1,1) &= \xi'\mathcal{I}_6,\end{aligned} \tag{A23}$$

where the factors $\xi' = [1/(ls)][1/(s+r)][l/(Q_-^2 s)]^{\kappa_-}\{s/[Q_+^2(s+r)]\}^{\kappa_+}$ cancel in Eq. (4.24). $\mathcal{I}_5,\ldots,\mathcal{I}_8$ are given by Eqs. (A19)–(A22), and l, s, r are given by Eq. (A17). Note that $\mathcal{I}_5,\ldots,\mathcal{I}_8$ are related to the hypergeometric functions of *three* arguments by Eq. (A5).

3. In region 6 we obtain from Eqs. (4.11), (4.12), (4.15) $\tan(S)=[1/Q_-,1/Q_+]$. For $t\in\tan(S)$ we have $1/Q_-<t<1/Q_+<-Q_-<-Q_+$, so that Eq. (4.20) can be written as

$$\begin{aligned}\tilde{I}(n,m_+,m_-) = (-1)^{2m_++m_-}&\int_{1/Q_-}^{1/Q_+} dt \\ &\times t^n(-t-Q_-)^{-\kappa_--m_-} \\ &\times(-t-Q_+)^{-\kappa_+-m_+}\left(t-\frac{1}{Q_-}\right)^{\kappa_--m_-} \\ &\times\left(\frac{1}{Q_+}-t\right)^{\kappa_+-m_+}.\end{aligned} \tag{A24}$$

Introducing the shorthands [in contrast to Eqs. (A7) and (A17)]

$$s=1/Q_+-1/Q_-,$$
$$m=-Q_--1/Q_+, \tag{A25}$$
$$r=-Q_++Q_-,$$

where obviously $s,m,r\geq 0$, the transformation $t'=(t-1/Q_-)/s$ yields

$$\begin{aligned}\tilde{I}(n,m_+,m_-)=&(-1)^m s^{1+\kappa_--m_-+\kappa_+-m_+}(s+m)^{-\kappa_--m_-}\\&\times(s+m+r)^{-\kappa_+-m_+}\int_0^1 dt'\left(st'+\frac{1}{Q_-}\right)^n\\&\times t'^{\kappa_--m_-}(1-t')^{\kappa_+-m_+}\\&\times\left(1-\frac{s}{s+m}t'\right)^{-\kappa_--m_-}\\&\times\left(1-\frac{s}{s+m+r}t'\right)^{-\kappa_+-m_+}.\end{aligned} \tag{A26}$$

For integer n, since $s/(s+m)<1$ and $s/(s+m+r)<1$, Eq. (A26) can be directly evaluated in terms of hypergeometric functions of *two* arguments.

APPENDIX B

We use two sets of material parameters for MBBA from the literature denoted by MBBA I [70] and MBBA II [71]. The quantities in the following table are the dielectric constants and conductivities parallel, $\varepsilon_\parallel$ and $\sigma_\parallel$, and perpendicular, $\varepsilon_\perp$ and $\sigma_\perp$, to the director, the viscous coefficients α_1, α_4, γ_1, γ_2, β, η_1, and η_2, the elastic constants K_{11} and K_{33}, and the Helfrich parameter ζ^2. A sample thickness of $d=100$ μm is assumed. We remark that both in [70] and [71] only the ratio $\sigma_\parallel/\sigma_\perp$ is given by 1.3 and 1.5, respectively. (The conductivities may differ from probe to probe up to an order of magnitude; the ratio is a more stable characteristic.) The value of $\sigma_\perp$ we used for MBBA II is found in [31]. The Helfrich parameter is defined by

$$\zeta^2=\left(1-\frac{\varepsilon_\parallel\sigma_\perp}{\varepsilon_\perp\sigma_\parallel}\right)\left(1-\frac{\gamma_1-\gamma_2}{2\eta_1}\frac{\varepsilon_\parallel}{\varepsilon_a}\right), \tag{B1}$$

where $\varepsilon_a=\varepsilon_\parallel-\varepsilon_\perp$.

The rescaling from dimensionless quantities for the mean number of jumps of the stochastic field is given by

$$\nu=\frac{1}{\tau_q}\alpha=\frac{4\pi\sigma_\parallel}{\varepsilon_\parallel}\alpha, \tag{B2}$$

which amounts to $\nu\simeq 150.7\,\alpha[\mathrm{s}^{-1}]$ for MBBA I and $\nu\simeq 359.4\,\alpha[\mathrm{s}^{-1}]$ for MBBA II. The time τ_q is defined by Eq. (B2). For voltages one obtains

$$\mathrm{U}=\sqrt{\frac{4\pi\eta\varepsilon_\parallel}{-\varepsilon_a\varepsilon_\perp\tau_q}}d\varepsilon, \tag{B3}$$

where $\eta=\gamma_1-(\gamma_1-\gamma_2)^2/4\eta_1$, which gives $\mathrm{U}\simeq 74.1\,\varepsilon[\mathrm{V}]$ for MBBA I and $\mathrm{U}\simeq 115.3\,\varepsilon[\mathrm{V}]$ for MBBA II.

APPENDIX C

The coefficients in Eq. (5.1) are explicitly given by

$$\frac{1}{T_q}=4\pi\frac{\sigma_\parallel k_x^2+\sigma_\perp k_z^2}{\varepsilon_\parallel k_x^2+\varepsilon_\perp k_z^2}, \tag{C1}$$

$$\sigma_H=\frac{(\sigma_\parallel\varepsilon_\perp-\varepsilon_\parallel\sigma_\perp)(k_x^2+k_z^2)}{\varepsilon_\parallel k_x^2+\varepsilon_\perp k_z^2}, \tag{C2}$$

$$a=\frac{1}{f}\left[\frac{1}{2}\frac{(\gamma_1-\gamma_2)k_x^4+(\gamma_1+\gamma_2)k_x^2k_z^2}{\alpha_1k_x^2k_z^2+(k_x^2+k_z^2)(\eta_1k_x^2+\eta_2k_z^2)}-\frac{\varepsilon_ak_x^2}{\varepsilon_\parallel k_x^2+\varepsilon_\perp k_z^2}\right], \tag{C3}$$

$$\frac{1}{T_\psi}=\Lambda_1-\Lambda_2E_t^2, \tag{C4}$$

where

$$f=\gamma_1-\frac{1}{4}\frac{[(\gamma_1-\gamma_2)k_x^2+(\gamma_1+\gamma_2)k_z^2]^2}{\alpha_1k_x^2k_z^2+(k_x^2+k_z^2)(\eta_1k_x^2+\eta_2k_z^2)}, \tag{C5}$$

$$\eta_1=\frac{1}{2}\left[\alpha_4-\gamma_2+\frac{1}{2}(\beta+\gamma_1)\right], \tag{C6}$$

$$\eta_2=\frac{1}{2}\left[\alpha_4+\gamma_2+\frac{1}{2}(\beta+\gamma_1)\right], \tag{C7}$$

$$\Lambda_1=\frac{1}{f}[K_{33}k_x^2+K_{11}k_z^2], \tag{C8}$$

$$\Lambda_2=\frac{1}{f}\left[\frac{\varepsilon_a\varepsilon_\perp(k_x^2+k_z^2)}{4\pi(\varepsilon_\parallel k_x^2+\varepsilon_\perp k_z^2)}\right]. \tag{C9}$$

Note that both $1/T_q$ and σ_H are proportional to $\sigma_\parallel$ if $\sigma_\parallel/\sigma_\perp=\mathrm{const}$.

[1] *Noise in Nonlinear Dynamical Systems*, Vols. 1–3, edited by F. Moss and P. V. E. McClintock (Cambridge University Press, Cambridge, 1989).

[2] S. Kai, T. Kai, M. Takata, and K. Hirakawa, J. Phys. Soc. Jpn. **47**, 1379 (1979).

[3] T. Kawakubo, A. Yanagita, and S. Kabashima, J. Phys. Soc. Jpn. **50**, 1451 (1981).

[4] H. R. Brand, S. Kai, and S. Wakabayashi, Phys. Rev. Lett. **54**, 555 (1985).

[5] S. Kai, T. Tamura, S. Wakabayashi, M. Imasaki, and H. R.

Brand, IEEE-IAS Conf. Records **85CH**, 1555 (1985).
[6] S. Kai, H. Fukunaga, and H. R. Brand, J. Phys. Soc. Jpn. **56**, 3759 (1987).
[7] S. Kai, H. Fukunaga, and H. R. Brand, J. Stat. Phys. **54**, 1133 (1989).
[8] U. Behn and R. Müller, Phys. Lett. **113A**, 85 (1985).
[9] R. Müller and U. Behn, Z. Phys. B **69**, 185 (1987).
[10] R. Müller and U. Behn, Z. Phys. B **78**, 229 (1990).
[11] A. Lange, R. Müller, and U. Behn, Z. Phys. B **100**, 477 (1996).
[12] M. M. Doyle and N. Sri Namachchiraya, J. Stat. Phys. **75**, 525 (1994).
[13] L. Arnold, SIAM (Soc. Ind. Appl. Math.) J. Appl. Math. **44**, 793 (1984).
[14] L. Arnold and P. Kloeden, SIAM (Soc. Ind. Appl. Math.) J. Appl. Math. **49**, 1242 (1989).
[15] L. Arnold and R. Z. Khasminskii, in *Proceedings of the Symposia in Pure Mathematics*, edited by M. C. Cranston and M. A. Pinsky (American Mathematical Society, Providence, 1995), Vol. 57, pp. 543–551.
[16] F. J. Dyson, Phys. Rev. **92**, 1331 (1953).
[17] B. Derrida and E. Gardner, J. Phys. (France) **45**, 1283 (1984).
[18] G. Benettin, Physica D **13**, 211 (1984).
[19] P. Markoš, Z. Phys. B **73**, 17 (1988); J. Phys.: Condens. Matter **1**, 4611 (1989); J. Stat. Phys. **70**, 889 (1993).
[20] R. Mainieri, Phys. Rev. Lett. **68**, 1965 (1992).
[21] A. Crisanti, G. Paladin, and A. Vulpiani, Phys. Rev. Lett. **71**, 789 (1993).
[22] A. Crisanti, G. Paladin, and A. Vulpiani, Phys. Rev. E **49**, R953 (1994).
[23] A. MacKinnon, J. Phys.: Condens. Matter **6**, 2511 (1994).
[24] R. Lima and M. Rahibe, J. Phys. A **23**, 781 (1990); **27**, 3427 (1994).
[25] *The Many-Body Problem. An Encyclopedia of Exactly Solved Models in One Dimension*, edited by D. C. Mattis (World Scientific, Singapore, 1993).
[26] A. Crisanti, G. Paladin, and A. Vulpiani, *Products of Random Matrices in Statistical Physics*, Springer Series in Solid-State Sciences, Vol. 104, edited by M. Cardona, P. Fulde, K. von Klitzing, and H.-J. Queisser (Springer-Verlag, Berlin, 1993).
[27] E. Dubois-Violette, P. G. de Gennes, and O. Parodi, J. Phys. (France) **32**, 305 (1971).
[28] E. Dubois-Violette, J. Phys. (France) **33**, 95 (1972).
[29] I. W. Smith, Y. Galerne, S. T. Lagerwall, E. Dubois-Violette, and G. Durand, J. Phys. Colloq. **36**, C1-237 (1975).
[30] L. Kramer and W. Pesch, in *Pattern Formation in Liquid Crystals*, edited by A. Buka and L. Kramer (Springer-Verlag, New York, 1996).
[31] E. Bodenschatz, W. Zimmermann, and L. Kramer, J. Phys. (France) **49**, 1875 (1988).
[32] L. Kramer and W. Pesch, Annu. Rev. Fluid Mech. **27**, 515 (1995).
[33] A. Lange, Ph.D. thesis, Universität Leipzig, 1993.
[34] V. I. Oseledec, Trans. Moscow Math. Soc. **19**, 197 (1968).
[35] G. Lauricella, Rend. Circ. Matem. **VII**, 111 (1893).
[36] P. Appell, J. Kampé de Fériet, *Fonctions Hypergéomé- triques et Hypersphériques, Polynomes d' Hermite* (Gauthier-Villars, Paris, 1926).
[37] H. Bateman, *Higher Transcendental Functions*, edited by A. Erdélyi (McGraw-Hill, New York, 1953), Vol. 1.
[38] V. E. Shapiro and V. M. Loginov, Physica A **91**, 563 (1978).
[39] H. R. Brand (private communication).
[40] H. Amm, U. Behn, N. Klöpper, and R. Stannarius (unpublished).
[41] H. Amm, U. Behn, Th. John, and R. Stannarius, Mol. Cryst. Liq. Cryst. Sci. Technol., Sect. A **304**, 525 (1997).
[42] Th. John, Diploma thesis, Universität Leipzig, 1997 (unpublished).
[43] M. V. Feigel'man and I. E. Staroselsky, Z. Phys. B **62**, 261 (1986).
[44] R. Müller, K. Lippert, A. Kühnel, and U. Behn, in *Self-organization in Activator Inhibitor Systems: Semiconductors, Gas Discharge and Chemical Active Media*, edited by H. Engel, F.-J. Niedernostheide, H.-G. Purwins, and E. Schöll (Wissenschaft und Technik Verlag, Berlin, 1996), pp. 246-251.
[45] R. Müller, K. Lippert, A. Kühnel, and U. Behn, Phys. Rev. E **56**, 2658 (1997).
[46] M. Kaiser and W. Pesch, Phys. Rev. E **48**, 4510 (1993).
[47] R. Graham, Phys. Rev. A **10**, 1762 (1974).
[48] J. Swift and P. C. Hohenberg, Phys. Rev. A **15**, 319 (1977).
[49] P. C. Hohenberg and J. Swift, Phys. Rev. A **46**, 4773 (1992).
[50] G. De Nigris, G. Nicolis, and H. Frisch, Phys. Rev. A **34**, 4211 (1986).
[51] M. Treiber and L. Kramer, Phys. Rev. E **49**, 3184 (1994).
[52] J. Viñals, E. Hernández-García, M. San Miguel, and R. Toral, Phys. Rev. A **44**, 1123 (1991).
[53] T. C. Elston and R. F. Fox, Phys. Rev. A **44**, 8403 (1991).
[54] E. Hernández-García, M. San Miguel, R. Toral, and J. Viñals, Physica D **61**, 159 (1992).
[55] E. Hernández-García, J. Viñals, R. Toral, and M. San Miguel, Phys. Rev. Lett. **70**, 3576 (1993).
[56] J. García-Ojalvo, A. Hernández-Machado, and J. M. Sancho, Phys. Rev. Lett. **71**, 1542 (1993).
[57] L. Ramirez-Piscina, A. Hernández-Machado, and J. M. Sancho, Phys. Rev. B **48**, 119 (1993).
[58] L. Ramírez-Piscina, A. Hernández-Machado, and J. M. Sancho, Phys. Rev. B **48**, 125 (1993).
[59] J. M. Sancho, A. Hernández-Machado, L. Ramírez-Piscina, and A. M. Lacasta, Acta Phys. Pol. B **24**, 733 (1993).
[60] P.-M. Lam and D. Bagayoko, Phys. Rev. E **48**, 3267 (1993).
[61] T. Yamada, Phys. Lett. A **161**, 489 (1992).
[62] T. Yamada, K. Fukushima, and H. Fujisaka, Physica A **204**, 755 (1994).
[63] C. Van den Broeck, J. M. R. Parrondo, J. Armero, and A. Hernández-Machado, Phys. Rev. E **49**, 2639 (1994).
[64] A. Becker and L. Kramer, Phys. Rev. Lett. **73**, 955 (1994).
[65] A. Becker and L. Kramer, Physica D **90**, 408 (1996).
[66] R. Graham and A. Schenzle, Phys. Rev. A **25**, 1731 (1982).
[67] A. Teubel, U. Behn, and A. Kühnel, Z. Phys. B **71**, 393 (1988).
[68] M. Treiber and L. Kramer, Mol. Cryst. Liq. Cryst. Sci. Technol., Sect. A **261**, 311 (1995).
[69] J. M. Deutsch, Phys. Rev. E **48**, R4179 (1993).
[70] N. V. Madhusudana, V. A. Raghunathan, and K. R. Sumathy Pramana, J. Phys. **28**, L311 (1987).
[71] W. J. A. Goossens, in *Advances in liquid crystals*, Vol. 3, edited by G. H. Brown (Academic Press, New York, 1978), p. 1.